

# Decentralized Robust Disturbance-Observer based LFC of Interconnected Systems

**Vafamand, Navid; Arefi, Mohammad Mehdi; Asemani, Mohammad Hassan; Dragicevic, Tomislav**

*Published in:*
IEEE Transactions on Industrial Electronics

*Link to article, DOI:*
10.1109/TIE.2021.3078352

*Publication date:*
2022

*Document Version*
Peer reviewed version

# Decentralized Robust Disturbance-Observer based LFC of Interconnected Systems

Navid Vafamand, Mohammad Mehdi Arefi, *Senior Member*, *IEEE*, Mohammad Hassan Asemani, and Tomislav Dragičević, *Senior Member, IEEE*

***Abstract*—This paper develops a novel decentralized controller for multi-area secondary load frequency control (LFC) of power systems. The proposed robust-adaptive approach estimates the external disturbance input and uncertainties, which are assumed to be matched with the control input. In this regard, a disturbance-observer state-feedback controller is designed. To offer a systematic approach, controller design conditions are derived in terms of linear matrix inequality (LMI) constraints. Thereby, for any given representation of the LFC area, the controller gains can be straightforwardly obtained by using numerical solvers. Moreover, in order to enhance the steady-state performance, the controller is modified through the heuristic genetic algorithm (GA). The controller design procedure is wholly offline and can be simply implemented. The developed decentralized approach does not need the information of the other areas, which reduces the cost and the number of measuring units. It is also robust against the power fluctuations of the load and renewable energy sources. To show the superiorities of the developed controller, four scenarios are considered. These scenarios comprise the aggregation of the photovoltaic, wind turbines, and electric vehicle (EV) to the power system. OPAL-RT experiments are given to verify the transient and steady-state performance and robustness of the proposed controller.**

***Index Terms*—Load frequency control, Decentralized control, Robust control, Disturbance observer, multi-area power systems, Genetic algorithm.**

## I. Introduction

ALTERNATING current (AC) power systems are inherently fragile against the inconsistency of load demand and generated power which causes undesired devotions in frequency and bus voltages [1]. This issue is getting worsen for the case of interconnected large-scale power systems in which single areas are connected by tie-lines [2]. In these systems, it is vital to properly regulate the frequency of each area as well as the inter-area tie-line to desired values. The issue of regulating the output real power of generating components in response to changes in AC power application frequency is called load frequency control (LFC) [3]. The LFC is vital for the proper operation of complex interconnected systems AC power systems.

The pioneer works on LFC were proportional-integral (PI) and proportional-integral-derivative (PID) controllers [4], which were tuned and improved by using soft computing optimization techniques, including heuristic [5], fuzzy [6], [7], and neural network [8]. However, as the size and intricacy of modern AC power applications are enlarged, the tuning of conventional PID controllers turns into an obstacle factor to design a proper controller for nonlinear and complicated systems. Thereby, advanced control methods were merged in the LFC, including, optimal control [9], [10], sliding mode control [11]–[14], robust $H_\infty$ control [15]–[18], and model predictive control [1], [19], [20]. Although such advanced control methods were successful in satisfying the desired performances, the unknown disturbance inputs are assumed to be norm-bounded with pre-known upper limits. Such a consideration may increase the controller conservativeness and LFC response osculation. Also, involving renewable energy sources with stochastic weather characteristics inputs obstacles utilizing the mentioned robust techniques. Therefore, instead of considering the pre-know upper limit of external disturbance inputs, in several control approaches, disturbance inputs are estimated and then compensated by an adaptive disturbance-observer-based control scheme. Although a disturbance-observer can be incorporated with several advanced control methods [21]–[23], for the secondary LFC issue, mainly it is merged with the sliding mode control [24]–[27]. Though, using sliding mode control provides a discontinuous control input law with chattering. As a result, the command input of the power elements may change very fast which they cannot respond adequately to this input law. A very few approaches present a disturbance observer-based smooth control law for the LFC of power systems. In [28], a disturbance-observer is used to estimate the power of renewable energy source powers and load power in a stand-alone power system. Then, an adaptive PI controller is suggested to regulate the frequency. However, the developed PI controller does not provide good performance, especially for the case high perturbed stand-alone power system. In [29] and [30], the external disturbance is estimated by an extended state observer (ESO) and a disturbance-observer, respectively. Then, a state

N. Vafamand, M.M. Arefi, and M.H. Asemani are with the School of Electrical and Computer Engineering, Shiraz University, Shiraz, Iran. (e-mails: {n.vafamand, arefi, asemani}@shirazu.ac.ir).

T. Dragičević is with the Department of Electrical Engineering, Technical University of Denmark, Lyngby, Denmark (e-mail: tomdr@elektro.dtu.dk).

feedback controller is designed. It is assumed that the tie-power is exactly known and the effect of renewable energy sources is not studied. Furthermore, controller gains are not designed systematically. In [31], the results of [28] are extended to interconnected systems, and the control gains are tuned by soft optimization methods. However, transient and steady-state performances are not theoretically investigated.

To sum up, this paper considers the decentralized robust-adaptive controller to regulate the frequency of multi-area power systems. The controller comprises state-feedback law and disturbance-observer to assure the transient performance of the closed-loop system. Also, a scalar modifying term is added to improve the steady-state performance. The controller gains are computed offline by using linear matrix inequality (LMI) and genetic algorithm (GA). The main contributions of this work are as follows: I) a novel controller structure for the multi-area LFC is proposed. In the proposed disturbance observer, all disturbance inputs are accumulated into a matched disturbance vector, which is estimated and rejected by a linear controller. This reduces the implementation burden and facilitates incorporating linear controller and disturbance observer. II) The closed-loop stability, as well as the transient and steady-state performances, are proved. Moreover, the GA is used to minimize the steady-state output error by tuning the weight of the estimated disturbance in the control law. III) the proposed controller does not require the information of the neighbor area frequency. Therefore, it is appliable whenever the communication between the neighbor areas is down. Furthermore, the effects of aggregating electric vehicle (EV) and renewable energy sources and different types of governors on the frequency deviation are studied. OPAL-RT results are provided to show the applicability and merits of the suggested advanced controller and the transient and steady-state performance of the AC microgrid (MG) power system deviation frequency response.

This paper is continued as follows: In Section II, the LFC problem for multi-area interconnected power systems (IMPS) is presented. In Section III, the linear robust disturbance observer-based controller is proposed. In Section IV, the theoretical stability analysis of the closed-loop system is performed. In Section V, the proposed controller is modified by GA. In Section VI, OPAL-RT experiments are provided and the results are compared with other approaches. Section VII ends this paper by evoking some concluding remarks and future perspectives.

## II. LFC Problem of Multi-area Systems

IMPS comprise several single areas each of which has non-linear and complex dynamics and their complexity is increased if numerous generators (G) and loads (LOs) are connected to them. These single areas are interconnected by tie-line and their operations affect each other. A typical multi-area power system is shown in Fig. 1. Generally, every single area comprises several power generators and energy storage systems, renewable energy sources, and loads. Some examples as shown in Fig. 1 are photovoltaic (PV), wind turbine (WT), diesel generator (DG), electric vehicle (EV), battery (BA), and loads.

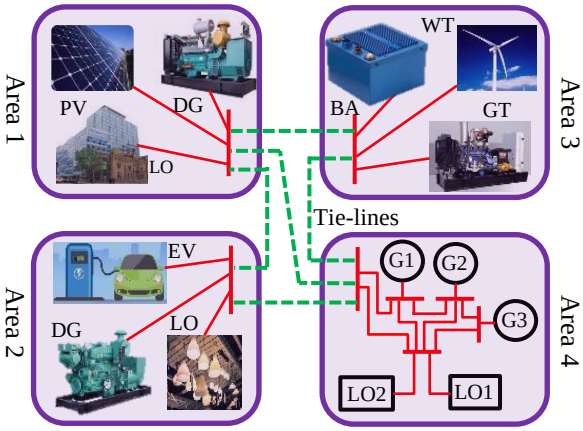


Fig. 1: Block diagram of a multi-area power system.

Although most of the power elements act high nonlinear, in the topic of secondary LFC, they are exposed to small load power demand changes and their dynamics can be characterized by linear models [31]. In other words, it is assumed that a proper primary controller is designed for each individual and in the secondary LFC, the command demand for each closed-loop system is designed. For power changes near the nominal operation, the response of the closed-loop systems to the command filter is modeled by a linear transfer function [2]. The block diagram of a single-area power system supplying power

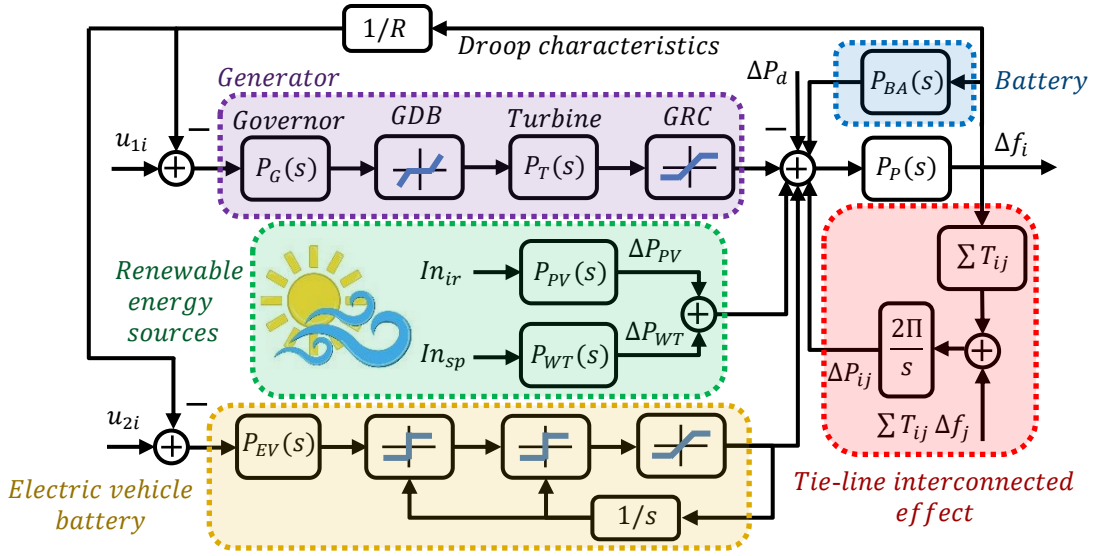


Fig. 2: The detailed $i$-th area of an interconnected power system.

to a single service area by a single generator is shown in Fig. 2. As can be seen in Fig. 2, the load change $\Delta P_d$ influences the single area power system frequency $\Delta f_i$ through the power machine transfer function $P_P(s)$. On the other hand, frequency variations of every single area affect the other interconnected area through the tie-lines. The tie-line interconnection effect is characterized by the synchronizing coefficients $T_{ij}$. The overall secondary LFC representation of generators comprises the transfer functions of the governor $P_G(s)$ and the turbine $P_T(s)$ and two nonlinear functions generation rate constraint (GRC) and governor dead band (GDB) [32]. Renewable energy PV and WT sources are modeled by transfer functions $P_{PV}(s)$ and $P_{WT}(s)$, respectively, actuated by sun irradiation and wind speed profiles $In_{ir}$ and $In_{sp}$ to produce $\Delta P_{PV}$ and $\Delta P_{WT}$ [1]. The considered EV is not near the full or empty state-of-charge (SOC) situation. Thereby, its complicated behavior can be modeled by the linear transfer function $P_{EV}(s)$ and some signum and saturation functions [4]. Finally, the battery is considered to be in the charging mode and represented by a linear transfer function [4]. The details for the transfer functions will be given in Section V.

In this paper, it is assumed that the solar irradiation and wind speed profiles and the load change are unknown. Moreover, it is assumed that the interconnected power fluctuations arose from the variations of the incremental frequency of other area $\Delta f_j$ are not measurable and known. Therefore, the conventional centralized and decentralized controllers that exploit the so-called area control error (ACE) are not applicable in this paper. The ACE is a function of $\Delta f_i$ and $\Delta P_{ij}$ and used as the input of the controller. Since in this paper, it is assumed that $\Delta f_j$ is unknown, the parameter $\Delta P_{ij}$ is unmeasurable and can be not considered in the control law. Consequently, there is no need to measure the frequency or power of the neighbor areas or communicate and share such information. This reduces the implementation and monitoring cost of the measuring units. Also, if the topology of the multi-area LFC system is changed, there is no need to alter the control action of each area. Additionally, avoiding the need for communication between neighbors, the proposed approach is inherently robust against cyber-attacks that could happen in the communication links. On the other hand, if the information of the neighbor areas is totally or partially available, the ACE can be used to reduce the amplitude of the control input command. Though, this issue is not considered in this paper. Ignoring the GBD and GRC nonlinearly functions [32] as well as the saturation and signum functions of the EV [4], the $i$-th area of the power system is represented by the following state-space form:

$$\dot{x}_i = (A_i + \Delta A_i)x_i + (B_i + \Delta B_i)u_i + E_i v_{1i} \quad (1)$$

where $x_i$, $u_i$, and $v_{1i}$ are the state, input, disturbance vectors whose dimension depends on the number and type of power elements installed in $i$-th area. $A_i(\Delta A_i)$ and $B_i(\Delta B_i)$ are the $i$-th area system and input (uncertainty)matrices. The state, control input, and disturbance vectors and matrices of (1) are obtained based on the topology and involving power elements of each area.

Consider that all uncertainties and mismatched disturbance inputs are incorporated into a matched disturbance input. In other words, all uncertainties and disturbance inputs on the system are accumulated into an artificial matched disturbance input. The artificial matched disturbance has the same effect on the system as the original disturbance $v_{1i}$. Thus, the system (1) can be re-written as follows:

$$\dot{x}_i = A_i x_i + B_i u_i + B_i v_{2i} \quad (2)$$

where $v_{2i}$ is the artificial matched disturbance. Although the disturbance vector $v_{2i}$ may not have a physical concept, but its estimation will be utilized in the control law to stabilize the original nonlinear LFC system of Fig. 2. To have a better understanding of $v_{2i}$, consider that the transfer functions of the state-space representations (1) and (2) are of the following forms, respectively:

$$Y_i = T_i(s)U_i + G_i(s)V_{1i} \quad (3)$$

$$Y_i = T_i(s)U_i + T_i(s)V_{2i} \quad (4)$$

where $Y_i$, $U_i$, $V_{1i}$, $V_{2i}$ are the Laplacian forms of the output, the control input, and the disturbance inputs of the LFC system, respectively, and $T_i(s)$ and $G_i(s)$ are the transfer functions from the control and disturbance inputs to the output. Comparing (3) with (4) reveals that $V_{2i} = \frac{G_i(s)}{T_i(s)} V_{1i}$. The system (4) is not needed to be implemented and the stability of $\frac{G_i(s)}{T_i(s)}$ is not important. However, it gives an insight into the relationship between the amplitude of disturbance inputs $V_{2i}$ and $V_{1i}$ by considering the norm of $\frac{G_i(s)}{T_i(s)}$. It is worthy to note that the uncertain linear systems (1) and (2) are only used to design the controller. Though, the controller is then applied to the original LFC system with nonlinearities.

Therefore, the goal is to design a decentralized controller $u_i$ for every single area so that it is robust against the unknown parameters accumulated in the external disturbance input $v_{2i}$ and regulates the real power of the generators and EVs to make the incremental change of frequency $\Delta f_i$ zero.

## III. DISTURBANCE-BASED STATE-FEEDBACK CONTROLLER

Designing a proper decentralized controller for the system (2) has three main challenges. I) The systems states $x_i$ are dependent on the unknown value of the external disturbance $v_i$. Therefore, to have a good closed-loop performance, it is necessary to compensate for the external disturbance by estimating it online. II) The state-space representation is subjected to inaccuracies and uncertainties of the system and input matrices. To minimize the tracking error, it is vital to consider the uncertainty terms in the controller design procedure. III) To achieve a fast closed-loop response, the conventional asymptotic stability should be replaced by exponential stability [33]. The first two challenges correspond to the steady-state performance, meanwhile, the last one is related to the transient performance. To deal with the above-mentioned issues, the disturbance observer [21]

$$\begin{aligned} \dot{z}_i &= -L_i(A_i x_i + B_i u_i + B_i \hat{v}_{2i}) \\ \hat{v}_{2i} &= z_i + L_i x_i \end{aligned} \quad (5)$$

and the state feedback controller

$$u_i = K_i x_i - \hat{v}_{2i} \quad (6)$$

are considered. In (5) and (6), $z_i$ and $\hat{v}_{2i}$ are the disturbance observer and estimation state vector, respectively, $L_i$ and $K_i$ are gains of the disturbance-observer and controller gains, which should be designed. To perform this, the closed-loop system based on (2) and (6) is as follows:

$$\dot{x}_i = (A_i + B_i K_i)x_i + B_i e_i \tag{7}$$

where $e_i = v_{2i} - \hat{v}_{2i}$ is the disturbance-observer estimation error. Thereby, considering (5) and (7) results into

$$\dot{e}_i = \dot{z}_i + L_i\dot{x}_i - \dot{v}_{2i} = -L_i B_i e_i + \dot{v}_{2i} \tag{8}$$

Defining the augmented vector $s_i = [x_i^T \;\; e_i^T]^T$ provides

$$\dot{s}_i = \begin{bmatrix} A_i + B_i K_i & B_i \\ 0 & -L_i B_i \end{bmatrix} s_i + \begin{bmatrix} 0 \\ \dot{v}_i \end{bmatrix} \tag{9}$$

In the following theorem, by considering the above-mentioned controller and disturbance observer the closed-loop stability is investigated.

**Theorem 1:** The augmented perturbed closed-loop system (9) defined based on the disturbance observer (5) and controller (6) is stable in-large if there exist LMI variable matrices $X_{1i} = X_{1i}^T$ and $P_{2i} = P_{2i}^T$, $M_i$, and $N_i$ so that the following LMI constraints hold:

$$X_{1i} > 0 \tag{10}$$

$$P_{2i} > 0 \tag{11}$$

$$\begin{bmatrix} \begin{Bmatrix} A_i X_{1i} + B_i N_i + X_{1i} A_i^T \\ + N_i^T B_i^T + \alpha_{1i} X_{1i} \end{Bmatrix} & B_i & 0 \\ B_i^T & \begin{Bmatrix} \alpha_{2i} P_{2i} - M_i B_i \\ - B_i^T M_i^T \end{Bmatrix} & P_{2i} \\ 0 & P_{2i} & -\beta_i I \end{bmatrix} < 0 \tag{12}$$

Then, the gains of the controller and disturbance-observer are computed by

$$L_i = M_i P_{2i}^{-1},\; K_i = N_i X_{1i}^{-1} \tag{13}$$

**Proof:** Consider the following Lyapunov candidate:

$$V = s_i^T P_i s_i \tag{14}$$

where $P_i = diag\{P_{1i}, P_{2i}\}$ and $P_{1i}$ and $P_{2i}$ are symmetric positive definite matrices. Taking the time derivative of (14) with respect to (9) results in

$$\begin{aligned} \dot{V} &= s_i^T P_i \dot{s}_i + \dot{s}_i^T P_i s_i + \alpha_i s_i^T P_i s_i - \alpha_i s_i^T P_i s_i \\ &= s_i^T \left( \begin{bmatrix} P_{1i} & 0 \\ 0 & P_{2i} \end{bmatrix} \begin{bmatrix} A_i + B_i K_i & B_i \\ 0 & -L_i B_i \end{bmatrix} \right. \\ &\quad + \begin{bmatrix} A_i + B_i K_i & B_i \\ 0 & -L_i B_i \end{bmatrix}^T \begin{bmatrix} P_{1i} & 0 \\ 0 & P_{2i} \end{bmatrix} \\ &\quad \left. + \alpha_i \begin{bmatrix} P_{1i} & 0 \\ 0 & P_{2i} \end{bmatrix} \right) s_i \\ &\quad - s_i^T \alpha_i \begin{bmatrix} P_{1i} & 0 \\ 0 & P_{2i} \end{bmatrix} s_i + \begin{bmatrix} 0 \\ \dot{v}_{2i} \end{bmatrix}^T \begin{bmatrix} 0 & 0 \\ 0 & I \end{bmatrix} \begin{bmatrix} P_{1i} & 0 \\ 0 & P_{2i} \end{bmatrix} s_i \\ &\quad + s_i^T \begin{bmatrix} P_{1i} & 0 \\ 0 & P_{2i} \end{bmatrix} \begin{bmatrix} 0 & 0 \\ 0 & I \end{bmatrix} \begin{bmatrix} 0 \\ \dot{v}_{2i} \end{bmatrix} \end{aligned} \tag{15}$$

where $\alpha_i = diag\{\alpha_{1i} I, \alpha_{2i} I\}$. Considering the fact that $W^T R + R^T W \le \beta W^T W + \beta^{-1} R^T R$ hold for any matrices $W$ and $R$ and $\beta > 0$, (15) is continued as

$$\begin{aligned} \dot{V} &\le s_i^T \left( \begin{bmatrix} P_{1i} & 0 \\ 0 & P_{2i} \end{bmatrix} \begin{bmatrix} A_i + B_i K_i & B_i \\ 0 & -L_i B_i \end{bmatrix} \right. \\ &\quad + \begin{bmatrix} A_i + B_i K_i & B_i \\ 0 & -L_i B_i \end{bmatrix}^T \begin{bmatrix} P_{1i} & 0 \\ 0 & P_{2i} \end{bmatrix} + \alpha_i \begin{bmatrix} P_{1i} & 0 \\ 0 & P_{2i} \end{bmatrix} \\ &\quad \left. + \beta_i^{-1} \begin{bmatrix} P_{1i} & 0 \\ 0 & P_{2i} \end{bmatrix} \begin{bmatrix} 0 & 0 \\ 0 & I \end{bmatrix} \begin{bmatrix} 0 & 0 \\ 0 & I \end{bmatrix} \begin{bmatrix} P_{1i} & 0 \\ 0 & P_{2i} \end{bmatrix} \right) s_i \\ &\quad - s_i^T \alpha_i \begin{bmatrix} P_{1i} & 0 \\ 0 & P_{2i} \end{bmatrix} s_i + \beta_i \dot{v}_{2i}^T \dot{v}_{2i} \end{aligned} \tag{16}$$

Now, if

$$\begin{aligned} &s_i^T \left( \begin{bmatrix} P_{1i} & 0 \\ 0 & P_{2i} \end{bmatrix} \begin{bmatrix} A_i + B_i K_i & B_i \\ 0 & -L_i B_i \end{bmatrix} \right. \\ &+ \begin{bmatrix} A_i + B_i K_i & B_i \\ 0 & -L_i B_i \end{bmatrix}^T \begin{bmatrix} P_{1i} & 0 \\ 0 & P_{2i} \end{bmatrix} + \alpha_i \begin{bmatrix} P_{1i} & 0 \\ 0 & P_{2i} \end{bmatrix} \\ &\left. + \beta_i^{-1} \begin{bmatrix} P_{1i} & 0 \\ 0 & P_{2i} \end{bmatrix} \begin{bmatrix} 0 & 0 \\ 0 & I \end{bmatrix} \begin{bmatrix} 0 & 0 \\ 0 & I \end{bmatrix} \begin{bmatrix} P_{1i} & 0 \\ 0 & P_{2i} \end{bmatrix} \right) s_i < 0 \end{aligned} \tag{17}$$

then,

$$\dot{V} < -\bar{\alpha}_i V + \beta_i \dot{v}_i^T \dot{v}_i \tag{18}$$

where $\bar{\alpha}_i = max\,(\alpha_{1i}, \alpha_{2i})$. Initially, the constraint (17) will be derived in terms of LMIs. To perform this, apply the Congruence lemma on (17). Thereby,

$$\begin{bmatrix} \begin{Bmatrix} P_{1i} A_i + P_{1i} B_i K_i + \\ A_i^T P_{1i} + K_i^T B_i^T P_{1i} \\ + \alpha_{1i} P_{1i} \end{Bmatrix} & P_{1i} B_i \\ B_i^T P_{1i}^T & \begin{Bmatrix} \alpha_{2i} P_{2i} + \beta_i^{-1} P_{2i} P_{2i} - \\ P_{2i} L_i B_i - B_i^T L_i^T P_{2i}^T \end{Bmatrix} \end{bmatrix} < 0 \tag{19}$$

Multiplying left and right sides of (19) by $diag\{P_{1i}^{-1}, I\}$ and defining $X_{1i} = P_{1i}^{-1}$, $N_i = K_i P_{1i}^{-1}$, and $M_i = P_{2i} L_i$ result that

$$\begin{bmatrix} \begin{Bmatrix} A_i X_{1i} + B_i N_i + X_{1i} A_i^T \\ + N_i^T B_i^T + \alpha_{1i} X_{1i} \end{Bmatrix} & B_i \\ B_i^T & \begin{Bmatrix} \alpha_{2i} P_{2i} + \beta_i^{-1} P_{2i} P_{2i} \\ - M_i B_i - B_i^T M_i^T \end{Bmatrix} \end{bmatrix} < 0 \tag{20}$$

Applying the Schur complement on (20) obtains the LMI (12). The proof is therefore finished. ■

## IV. STABILITY ANALYSIS AND IMPLEMENTATION OF DEVELOPED CONTROLLER

Theorem 1 presents sufficient conditions of the disturbance-observer-based controller in terms of LMIs. In this section, rigorous stability analysis will be performed.

Solving the ordinary inequality (18), provides [34]

$$V(t) < e^{-\alpha t} V(0) + \beta \int_0^t e^{-\alpha \tau}\, \dot{v}_i^T(t-\tau)\dot{v}_i(t-\tau) d\tau \tag{21}$$

Substituting (14) into (21), results into

$$\begin{aligned} s_i^T(t) P_i s_i(t) &< e^{-\alpha t} s_i^T(0) P_i s_i(0) \\ &\quad + \beta \int_0^t e^{-\alpha \tau}\, \dot{v}_i^T(t-\tau)\dot{v}_i(t-\tau) d\tau \end{aligned} \tag{22}$$

Applying some simplifications on (22), provides

$$\begin{aligned} \lambda_{min}(P_i)\|s_i(t)\|_\infty^2 &\le e^{-\alpha t}\lambda_{max}(P_i)\|s_i(0)\|_\infty^2 \\ &\quad + \beta |\dot{v}_i^T(t-\tau)\dot{v}_i(t-\tau)| \int_0^t e^{-\alpha\tau} d\tau \\ &\le e^{-\alpha t}\lambda_{max}(P_i)\|s_i(0)\|_\infty^2 + \frac{\beta}{\alpha}\|\dot{v}_i(t)\|_\infty^2 \end{aligned} \tag{23}$$

From (23), one concludes that

$$\begin{aligned} \|s_i(t)\|_\infty &\le e^{-\frac{\alpha}{2}t} \sqrt{\frac{\lambda_{max}(P_i)}{\lambda_{min}(P_i)}} \|s_i(0)\|_\infty \\ &\quad + \sqrt{\frac{\beta}{\alpha \lambda_{min}(P_i)}} \|\dot{v}_i(t)\|_\infty \end{aligned} \tag{24}$$

Relation (24) reveals that the system states are bounded for all time; because $\|s_i(0)\|_\infty$ and $\|\dot{v}_i(t)\|_\infty$ are bounded. Additionally, as time goes $\infty$, the first term of the right-hand side

of (24) converges to zero. This means that the system augmented states are ultimately bounded as

$$\lim_{t\to\infty}\|s_i(t)\|_\infty \le \sqrt{\frac{\beta}{\alpha\lambda_{min}(P_i)}}\|\dot{v}_i(t)\|_\infty \quad (25)$$

Though, the upper bound of the systems states $x_i$ are more important than the augmented states $s_i(t)$. Additionally, the special structure of the dynamics (7) and (8) enables us to assure a smaller upper bound of the system states. Similar to the procedure (21)-(25), from the dynamics (8), one concludes

$$\lim_{t\to\infty}\|e_i(t)\|_\infty = \sqrt{\frac{1}{\sigma_{min}(L_iB_i)}}\|\dot{v}_i(t)\|_\infty \quad (26)$$

Also, from the dynamics (7), one concludes

$$\lim_{t\to\infty}\|x_i(t)\|_\infty = \sqrt{\frac{\sigma_{max}(B_i)}{\sigma_{min}(A_i+B_iK_i)}}\|e_i(t)\|_\infty \quad (27)$$

Merging (26) and (27) results in

$$\lim_{t\to\infty}\|x_i(t)\|_\infty = \sqrt{\frac{\sigma_{max}(B_i)}{\sigma_{min}(A_i+B_iK_i)\sigma_{min}(L_iB_i)}}\|\dot{v}_i(t)\| \quad (28)$$

The ultimate upper bound of the system states is dependent on the eigenvalues of stable matrices $A_i+B_iK_i$ and $L_iB_i$. Since the exponential stability with the decay rates $\alpha_{1i}$ and $\alpha_{2i}$ are considered in (12), the Eigenvalues of the matrices $A_i+B_iK_i$ and $L_iB_i$ are smaller than $\alpha_{1i}/2$ and $\alpha_{2i}/2$, respectively. Moreover, (25) shows that the parameter $\beta_i$ affects the bounds, such that smaller values of $\beta_i$ result in smaller ultimately upper bounds.

## V. Improving Steady-State Performance

As discussed in Section II, the LFC system contains the disturbance term $E_iv_{1i}$ in (1) and it is then estimated by the term $B_iv_{2i}$. Although in Sections III and IV, it is proved the overall-controller theoretically assures the closed-loop stability, the controller still suffers a mismatch between the terms $E_iv_{1i}$ and $B_iv_{2i}$, which affects the steady-state performance. To solve this issue, the disturbance observer (5) is modified as follows:

$$\begin{aligned}\dot{z}_i &= -L_i(A_ix_i+B_iu_i+B_i\hat{v}_{2i})\\ \hat{v}_{2i} &= z_i+L_ix_i\\ u_i &= K_ix_i-\alpha_i\hat{v}_{2i}\end{aligned} \quad (29)$$

where $\alpha_i$ is a tuning design scalar. The trivial value for $\alpha_i$ is one, which assures closed-loop stability. However, it is possible to choose a suitable value for that to improve the disturbance estimation. The rationale behind the modified disturbance observer-based controller (29) is that the role of the estimated disturbance $\hat{v}_{2i}$ is modified to avoid the mismatch between the real values $v_{1i}$ and $v_{2i}$ in (1) and (2). To select $\alpha_i$, heuristic approaches can be beneficial. To perform a heuristic algorithm, the objective function is defined as

$$J_1 = \int_0^\infty \Delta f(\tau)^2 d\tau \quad (30)$$

The heuristic algorithm is performed offline and with any kind of disturbance input. In other words, the way of selecting the disturbance in (1) does not affect the disturbance observer (29). The overall procedure of calculating disturbance observer-based controller gain matrices is shown in Fig. 3. As can be seen in Fig. 3, for each of the single area power systems, the state-space representation for the secondary LFC is derived. Then, the system matrices are utilized in Theorem 1 and the controller and disturbance-observer gains are obtained numerically using the LMI toolbox, Yalmip toolbox, etc. After that choose a constant disturbance power and apply the heuristic approach with the objective function (30) to find the modifying term of the disturbance observer. It is worthy to mention that the feasibility of LMIs of Theorem 1 guarantees the closed-loop stability, theoretically, as it is evident from (24) and (28). Moreover, the Yalmip toolbox and the genetic algorithm (GA) are used. The individuals in the GA are continuous character strings, called chromosomes. The GA starts with a random definition of the initial population of individuals. The quality of each individual is evaluated by the fitness function. After that, some individuals are selected as parents to create offspring. This task is performed by the crossover operator which produces one or two offsprings by mixing two selected parents. Also, the mutation operator is considered to escape from the local minimum. After these steps, the new population is replaced with the old population. If stopping criteria isn't satisfied, then the algorithm will be continued by checking the fitness of the new population. Finally, whenever the stopping criteria are met, the candidate individual with the highest fitness will be selected as the output of GA. The details of performing the GA can be found in [35], [36].

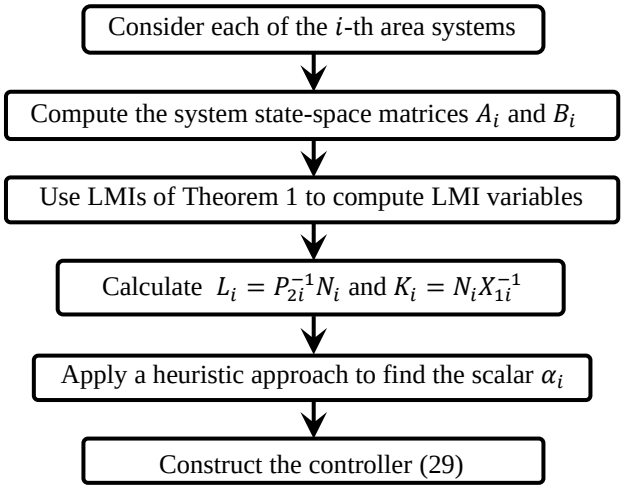


Fig. 3. The block diagram of controller design.

Fig. 4 illustrates the closed-loop system comprising $i$-th area power system and the proposed controller. The disturbance observer block uses the $i$-th area power system states to estimate the matched external disturbance and by deploying the estimated value and the system states, the control command to change the power of the controllable elements for the secondary LFC is computed. The proposed control approach can be implemented online without any major computational burden.

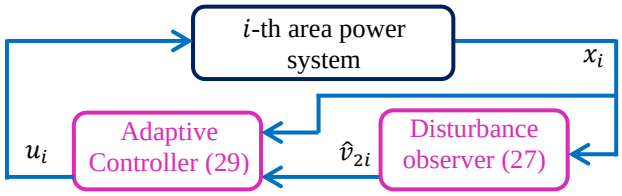


Fig. 4. The overall implementation of the proposed approach.

## VI. HIL OPAL-RT RESULTS

In this section, several scenarios are considered for the IMPS by using different types of governors and generators and ignoring and including renewable energy sources and EVs. The GRC of $10\%\text{min}^{-1}$ (i.e. $0.0017\ p.u.$) for the rising and falling generation of thermal units; and, $270\%\text{min}^{-1}$ (i.e. $0.045\ p.u.$) for the rising generation and $360\%\text{min}^{-1}$ (i.e. $0.06\ p.u.$) for the falling generation of hydro units are considered [37]. In order to implement the GDB nonlinearity, the approach of [38] with $N_1 = 0.8$ and $N_2 = -0.2$ is considered. Finally, the saturation functions of the EV are chosen such that the total energy of the EV is kept within $E_{min} = 0.8\ p.u.$ and $E_{max} = 0.95\ p.u.$ with the inverter capacity limit $\mu_e = 0.025\ p.u.$ and the power ramp rate limit $\delta_e = 0.01\ p.u.$ [39]. For all considered scenarios are tested by a HiL OPARL-RT simulator, as shown in Fig. 5 to provide more realistic results. In Scenario 1, the proposed is compared with state-of-the methods. And, scenarios 2-4, more complex multi-area systems are considered.


Fig. 5. The real-time simulation setup for testing the control approach.

**Scenario 1.** The goal of this scenario is to investigate the effect of the GA on the transient and steady-state performance of the frequency deviation. To perform this, a one-area LFC system is considered as follows [32]:

$$P_P = \frac{K_P}{T_P S + 1}, P_G = \frac{1}{T_G S + 1}, P_T = \frac{1}{T_T S + 1} \quad (31)$$

where $K_p = 120$, $T_p = 20$, $T_G = 0.08$, $T_T = 0.3$, $R = 2.4$, and a step signal with the amplitude $0.5\ p.u.$ for the load is considered. Initially, for the dynamics (31), the controller and disturbance observer gains are calculated and then, the GA is applied. The final values of the gains and modifying term are given in Appendix A (i.e. relation (36)). To evaluate the performance of the original and modifying controllers, the time-varying load profile is considered as:

$$\begin{cases} 0.1 & 0 \le t < 2 \\ 0.4 & 2 \le t < 4 \\ 0.8 & \text{for} \quad 4 \le t < 6 \\ 0.6 + 0.3\sin(50\pi t) & 6 \le t < 8 \\ 0.4 + 0.1 \times randn(t) & 8 \le t < 10 \end{cases} \quad (32)$$

where $randn(t)$ is a zero-mean white noise with the covariance 1. The considered profile (32) contains the fast-changing load profile $0.3\sin(50\pi t)$ and the stochastic behavior $0.1 \times randn(t)$ both of which have the amplitude variation $0.6\ p.u.$. The power load demand profile (32) is plotted in Fig. 6(a). The closed-loop frequency deviation and control input are shown in Figs. 6(b)-(c). As can be seen in Fig. 6(b), both controllers avoid instability in the frequency. However, for a large demand load power, the original controller does not provide a good steady-state system response. Though, by using the GA, the modified controller is able to effectively compensate for the step, fast variation, and stochastic loads.

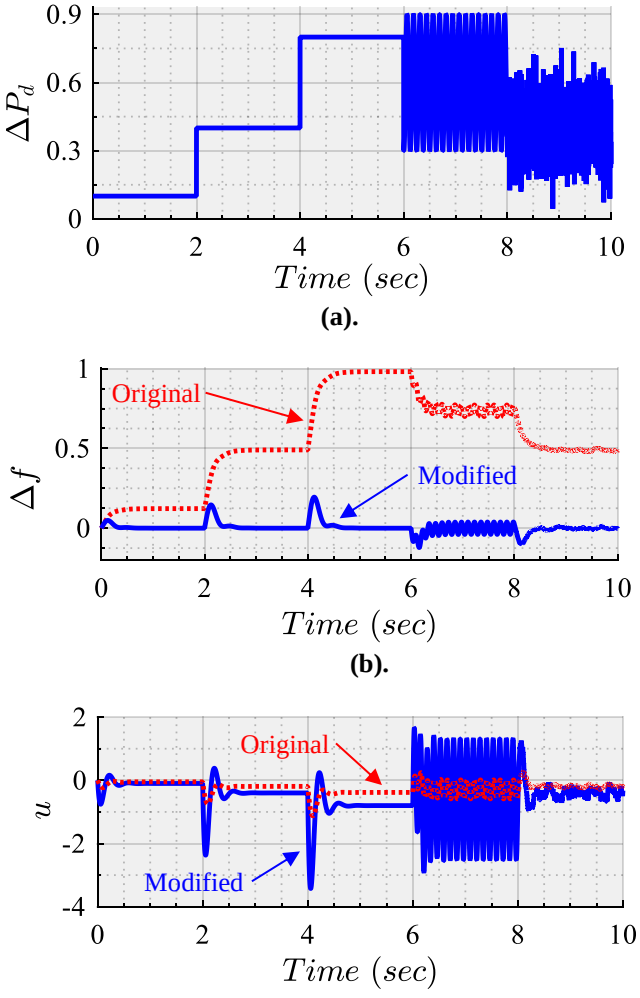


Fig. 6: Frequency response of Scenario 1 (the modified disturbance observer-based controller by the solid blue line and the original observer-based controller by the dotted red line): **(a).** $\Delta P_d$, **(b).** $\Delta f$, and **(c).** $u$.

**Scenario 2.** In this scenario, a two-area IMPS is considered and the results of the proposed controller are compared with the state-of-the-art controllers suggested for the secondary LFC system. In each area of the IMPS, a hydraulic governor with a non-reheated turbine is involved. Their and power system transfer functions are of the following form [32]:

$$P_{Pi} = \frac{K_{Pi}}{T_{Pi} S + 1}, P_{Gi} = \frac{1}{T_{Gi} S + 1}, P_{Ti} = \frac{1}{T_{Ti} S + 1} \quad (33)$$

where the values of the parameters of IMPS areas 1 and 2 are given in Table I. Also, the load demand is considered to a step-change with a period of 2 seconds, as shown in Fig. 7(a). The load demand changes in the range of 0.1 to $0.65\ p.u.$, which is a large range of variation. The step-change load demand is a widely considered disturbance in the LFC system [15], [16]. Though, it is shown in [40] and Scenario 1 that the robust $H_\infty$ scheme is able to reject stochastic power demand changes.

The proposed controller with the characteristics given in Appendix A (i.e. relation (36)) is compared with the robust $\mu$-synthesis controller [15], the disturbance observer-based fault-

tolerant controller [26], and the second-order disturbance observer-based linear controller [31]. The robust $\mu$-synthesis approach [15] provides a robust controller without estimating the disturbance input. Though, the controller uses a high order transfer function as the controller block to assure the robust-stability (i.e. the closed-loop stability in the presence of uncertainty) and the good-tracking (i.e. transient and steady-state closed-loop system response in the presence of external disturbance). The disturbance observer-based fault-tolerant controller estimates the disturbance input, which can be mismatched with the control input. The approach of [26] uses the information of the frequency and power of the neighbor areas to regulate the frequency of each local area. However, that control law is implemented with the same assumption of the proposed approach, in which, the frequency and power of other areas are not available. In [31], a fixed-structure second-order disturbance observer is used to estimate the power load demand. Then, a fixed-structure linear controller which the states of the disturbance observer is developed to make the LFC system a pure linear cascaded integration process.

Real-time simulations verify that the proposed approach improves both the transient and steady-state response, as evident from Fig. 7(b). Moreover, the amplitude of the control input command for the proposed approach is smaller than the other approaches, which reduces the fuel consumption and increases the lifetime of the generator. Although the approach of [15] does not need the information of the other neighbor areas, it cannot reject the disturbance completely and compensates it with the expense of the high control input commands. The disturbance observer-based approach [26] requires the information of other areas and if this information is not available or attacked, the controller performance degrades. Furthermore, the approach of [31] does not use the information of the LFC system dynamics in the controller design procedure, which results in the simultaneous estimation of the system dynamics and the external disturbance. This degrades the transient performance. These issues are handled by the proposed approach, which compensates for the external disturbances and requires no neighbor information, which avoids the issue of cyber-attacks of areas communications. Though, the proposed approach is still vulnerable to attacks occur in each area.

Table I: IMPS parameters values of areas 1 and 2 [32].

| Parameter | Value | Parameter | Value |
|---|---|---|---|
| $K_{P1}, K_{P2}$ | 120 $s$ | $T_{T1}, T_{T2}$ | 0.3 $s$ |
| $T_{P1}, T_{P2}$ | 20 $s$ | $R_1, R_2$ | 2.4 $Hz/p.u.$ |
| $T_{G1}, T_{G2}$ | 0.08 $s$ | $T_{12}, T_{21}$ | $0.545, -0.545$ $p.u.$ |

The interconnected power between the areas is given in Fig. 7(e). Since the tie-line power and the frequency of the neighbor area are assumed to be not available, the controller cannot regulate the interconnected power to keep it as small as possible. Moreover, to quantitively compare the results of this paper with [15], [26], and [31], Table II is given. In this Table, the integral of absolute error (IAE) and integral of squared error (ISE) are provided, which reveal that the frequency deviation indices based on the proposed approach outperform those of [15], [26], and [31].

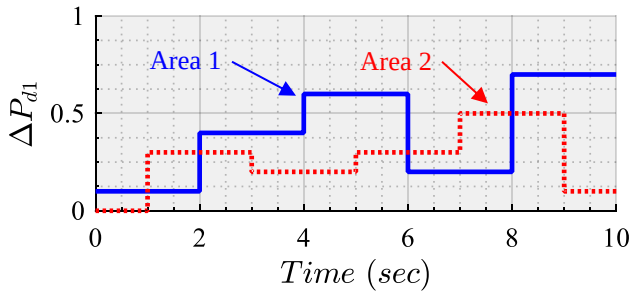


**(a).**

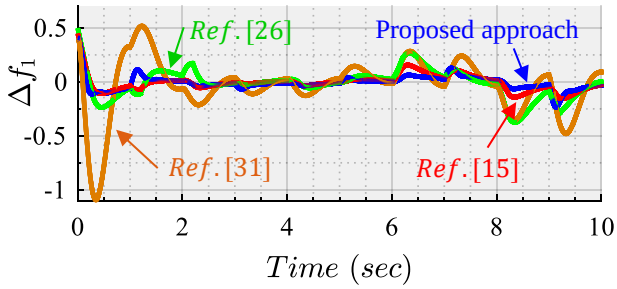


**(b).**

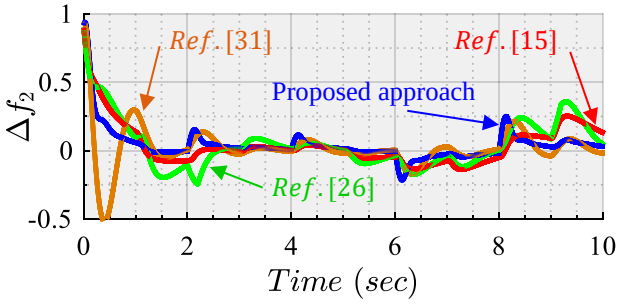


**(c).**

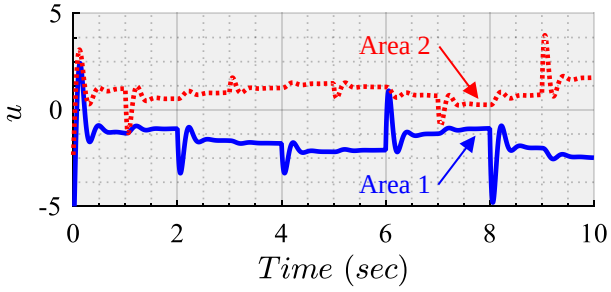


**(d).**

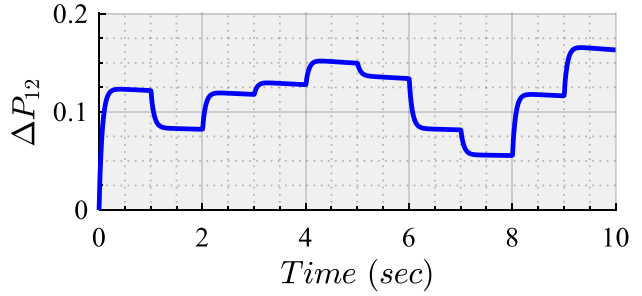


**(e).**

Fig. 7: Frequency response of Scenario 2: **(a).** $\Delta P_{di}$ **(b).** $\Delta f_1$, **(c).** $\Delta f_2$, **(d).** $u_i$ and **(e).** $\Delta P_{12}$.

Table II. The indices of frequency deviation for Scenario 2.

| | Area 1 | | Area 2 | |
|---|---|---|---|---|
| | IAE | ISE | IAE | ISE |
| Prop. App. | 453.7760 | 42.2263 | 645.3550 | 159.5544 |
| Ref. [15] | 521.5395 | 55.2575 | 1006.01 | 236.1479 |
| Ref. [26] | 944.2860 | 176.8627 | 1273.43 | 314.5324 |
| Ref. [31] | 1666.52 | 667.9709 | 1435.08 | 482.0177 |

**Scenario 3.** In this scenario, a four-area IMPS is considered. Areas 1 and 2 are the same as Scenario 2. Area 3 comprises a hydraulic governor with a hydro turbine and PV modeled as follows [32]:

$$P_{Gi} = \frac{1}{T_{Gi}S+1}, P_{Ti} = \frac{1-T_{Wi}S}{1+0.5T_{Wi}S}, P_{PVi} = \frac{1}{T_{PVi}S+1} \quad (34)$$

Also, Area 4 involves a Battery, EV, and WT, modeled as below [32]:

$$P_{BAi} = \frac{1}{T_{BAi}S+1}, P_{EVi} = \frac{1}{T_{Evi}S+1}, P_{WTi} = \frac{1}{T_{WTi}s+1} \quad (35)$$

where the values of the LFC parameters are given in Table III.

Table III: IMPS parameters values of areas 3 and 4 [32].

| Parameter | Value | Parameter | Value |
|---|---|---|---|
| $T_{G3}$ | $0.08\ s$ | $R_3$ | $2.82\ \mathrm{Hz}/p.u.$ |
| $T_{W3}$ | $1\ s$ | $T_{13}, T_{31}$ | $0.25, -0.25\ p.u.$ |
| $T_{P3}$ | $6\ s$ | $T_{12}, T_{21}$ | $0.2, -0.2\ p.u.$ |
| $K_{P3}$ | $120\ s$ | $T_{23}, T_{32}$ | $0.12, -0.12\ p.u.$ |
| $T_{PV3}$ | $1.8\ s$ | $T_{EV4}$ | $1\ s$ |
| $T_{WT4}$ | $1.5\ s$ | $R_4$ | $2.5\ \mathrm{Hz}/p.u.$ |
| $T_{BA4}$ | $0.1\ s$ | $T_{14}, T_{41}$ | $0.15, -0.15\ p.u.$ |
| $T_{P4}$ | $7\ s$ | $T_{24}, T_{42}$ | $0.1, -0.1\ p.u.$ |
| $K_{P4}$ | $100\ s$ | $T_{34}, T_{43}$ | $0\ p.u.$ |

Fig. 8 depicts the frequency responses of all areas with the initial conditions $\Delta f_1(0) = 1$, $\Delta f_2(0) = 0.5$, $\Delta f_3(0) = 0.1$, and $\Delta f_4(0) = 0.5$.

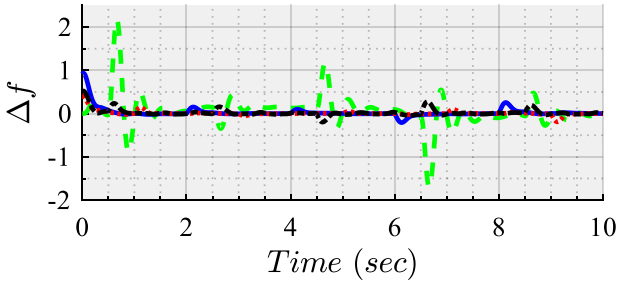


**(a).**

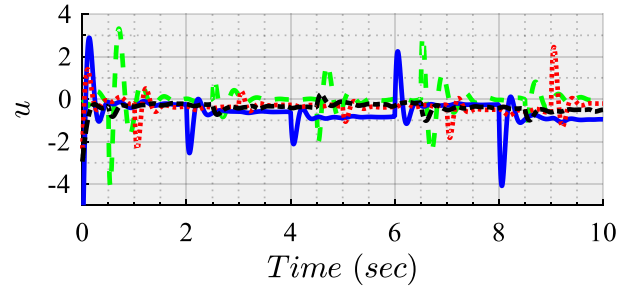


**(b).**

Fig. 8: Frequency response of Scenario 3 (Area 1 by the solid blue line, Area 2 by the dotted red line, Area 3 by the dashed green line, and Area 4 by the dashed-dotted black line): **(a).** $\Delta f_i$, **(b).** $u_i$.

Since the hydraulic governor with the hydro turbine acts as a non-minimum phase system, stabilizing the third area is a hard task. Thereby, the frequency deviation of the third area is higher than the two other ones. Though the controller not only stabilizes the third area in the presence of load power demand step changes and the power fluctuations of the photovoltaic but also the frequency deviation converges zero. Moreover, Areas 1 and 2 are able to effectively compensate for the high-frequency deviations of Area 3. Furthermore, the effect of the wind turbine is compensated by the EV aggregated in the LFC system and the battery.

## VII. Conclusion

In this paper, the problem of robust decentralized LFC for multi-area AC power applications was studied. The robust closed-loop stability, disturbance rejection, and transient and steady-state performances were used in the controller design procedure and the controller gains for each area were found offline by the means of LMIs and GA. In the OPAR-RT results and scenarios, several issues were studied, including renewable energy power fluctuation, load demand power changes, non-minimum phase generators, receiving no information from the other areas. The results showed that the proposed controller was able to effectively regulate the frequency of each area. Though, the proposed linear approach is effective when the nonlinearities are not significant and it cannot control the value of interconnected power of areas. For future work, considering state-observers and actuator faults makes the suggested approach more robust and practical. Moreover, optimal control of the batteries and evaluating the efficiency of the proposed approach against cyber-attacks are of great importance. Furthermore, study the optimal dispatch of tie-line and voltage of the power system are interesting topics.

## APPENDIX A

Based on the models of the generators, actuators, battery, and EV, the overall transfer functions of the open-loop system of each area can be obtained. Then, in order to derive the state-space representation of each area, MATLAB software is utilized via the command "ss" with the option "minimal". Then, the Yalmip third-party solver and the GA are used to calculate the following gains of each area controllers:

- Areas 1 and 2:

$$K_1 = K_2 = [-31.5316 \quad -8.0713 \quad 10.2135]$$
$$L_1 = L_2 = [-8.0667 \quad 2.0725 \quad -4.1754] \quad (36)$$
$$\alpha_1 = \alpha_2 = -36.665$$

- Area 3:

$$K_3 = [-31.6136 \quad 47.2774 \quad 13.1922]$$
$$L_3 = [-0.4944 \quad 3.7445 \quad -6.6110] \quad (37)$$
$$\alpha_3 = 712.53$$

- Area 4:

$$K_4 = [-10.9425 \quad -7.3853 \quad -5.5568]$$
$$L_4 = [188.9674 \quad -49.9015 \quad -81.9024] \quad (38)$$
$$\alpha_4 = 0.05223$$

## REFERENCES


[1] N. Vafamand, M. H. Khooban, T. Dragicevic, J. Boudjadar, and M. H. Asemani, "Time-Delayed Stabilizing Secondary Load Frequency Control of Shipboard Microgrids," *IEEE Syst. J.*, vol. 13, no. 3, pp. 3233–3241, 2019, doi: 10.1109/JSYST.2019.2892528.

[2] S. Trip and C. De Persis, "Distributed Optimal Load Frequency Control with Non-Passive Dynamics," *IEEE Trans. Control Netw. Syst.*, vol. 5, no. 3, pp. 1232–1244, Sep. 2018, doi: 10.1109/TCNS.2017.2698259.

[3] R. Shankar, S. R. Pradhan, K. Chatterjee, and R. Mandal, "A comprehensive state of the art literature survey on LFC mechanism for power system," *Renew. Sustain. Energy Rev.*, vol. 76, pp. 1185–1207, Sep. 2017, doi: 10.1016/j.rser.2017.02.064.

[4] H. Fan, L. Jiang, C.-K. Zhang, and C. Mao, "Frequency regulation of multi-area power systems with plug-in electric vehicles considering communication delays," *IET Gener. Transm. Distrib.*, vol. 10, no. 14, pp. 3481–3491, Nov. 2016, doi: 10.1049/iet-gtd.2016.0108.

[5] M. R. Khalghani, M. H. Khooban, E. Mahboubi-Moghaddam, N. Vafamand, and M. Goodarzi, "A self-tuning load frequency control strategy for microgrids: Human brain emotional learning," *Int. J. Electr. Power Energy Syst.*, vol. 75, pp. 311–319, Feb. 2016, doi: 10.1016/j.ijepes.2015.08.026.

[6] N. Jalali, H. Razmi, and H. Doagou-Mojarrad, "Optimized fuzzy self-tuning PID controller design based on Tribe-DE optimization algorithm and rule weight adjustment method for load frequency control of interconnected multi-area power systems," *Appl. Soft Comput.*, vol. 93, p. 106424, Aug. 2020, doi: 10.1016/j.asoc.2020.106424.

[7] A. Dokht Shakibjoo, M. Moradzadeh, S. Z. Moussavi, and L. Vandevelde, "A Novel Technique for Load Frequency Control of Multi-Area Power Systems," *Energies*, vol. 13, no. 9, p. 2125, Apr. 2020, doi: 10.3390/en13092125.

[8] A. Fathy and A. M. Kassem, "Antlion optimizer-ANFIS load frequency control for multi-interconnected plants comprising photovoltaic and wind turbine," *ISA Trans.*, vol. 87, pp. 282–296, Apr. 2019, doi: 10.1016/j.isatra.2018.11.035.

[9] S. Trip, M. Cucuzzella, C. De Persis, A. van der Schaft, and A. Ferrara, "Passivity-Based Design of Sliding Modes for Optimal Load Frequency Control," *IEEE Trans. Control Syst. Technol.*, vol. 27, no. 5, pp. 1893–1906, Sep. 2019, doi: 10.1109/TCST.2018.2841844.

[10] M. W. Siti, D. H. Tungadio, Y. Sun, N. T. Mbungu, and R. Tiako, "Optimal frequency deviations control in microgrid interconnected systems," *IET Renew. Power Gener.*, vol. 13, no. 13, pp. 2376–2382, Oct. 2019, doi: 10.1049/iet-rpg.2018.5801.

[11] G. Rinaldi, M. Cucuzzella, and A. Ferrara, "Third Order Sliding Mode Observer-Based Approach for Distributed Optimal Load Frequency Control," *IEEE Control Syst. Lett.*, vol. 1, no. 2, pp. 215–220, Oct. 2017, doi: 10.1109/LCSYS.2017.2712564.

[12] X. Su, X. Liu, and Y.-D. Song, "Event-Triggered Sliding-Mode Control for Multi-Area Power Systems," *IEEE Trans. Ind. Electron.*, vol. 64, no. 8, pp. 6732–6741, Aug. 2017, doi: 10.1109/TIE.2017.2677357.

[13] H. Li, X. Wang, and J. Xiao, "Adaptive Event-Triggered Load Frequency Control for Interconnected Microgrids by Observer-Based Sliding Mode Control," *IEEE Access*, vol. 7, pp. 68271–68280, 2019, doi: 10.1109/ACCESS.2019.2915954.

[14] A. E. Onyeka, Y. Xing-Gang, Z. Mao, B. Jiang, and Q. Zhang, "Robust decentralised load frequency control for interconnected time delay power systems using sliding mode techniques," *IET Control Theory Appl.*, vol. 14, no. 3, pp. 470–480, Feb. 2020, doi: 10.1049/iet-cta.2019.0809.

[15] K. Torabi-Farsani, M. H. Asemani, F. Badfar, N. Vafamand, and M. H. Khooban, "Robust Mixed μ-Synthesis Frequency Regulation in AC Mobile Power Grids," *IEEE Trans. Transp. Electrification*, vol. 5, no. 4, pp. 1182–1189, Dec. 2019, doi: 10.1109/TTE.2019.2960637.

[16] H. Zhang, J. Liu, and S. Xu, "H-Infinity Load Frequency Control of Networked Power Systems via an Event-Triggered Scheme," *IEEE Trans. Ind. Electron.*, vol. 67, no. 8, pp. 7104–7113, Aug. 2020, doi: 10.1109/TIE.2019.2939994.

[17] C. J. Ramlal, A. Singh, S. Rocke, and M. Sutherland, "Decentralized Fuzzy H∞-Iterative Learning LFC With Time-Varying Communication Delays and Parametric Uncertainties," *IEEE Trans. Power Syst.*, vol. 34, no. 6, pp. 4718–4727, Nov. 2019, doi: 10.1109/TPWRS.2019.2917613.

[18] A. D. Rosaline and U. Somarajan, "Structured H-Infinity Controller for an Uncertain Deregulated Power System," *IEEE Trans. Ind. Appl.*, vol. 55, no. 1, pp. 892–906, Jan. 2019, doi: 10.1109/TIA.2018.2866560.

[19] J. Liu, Q. Yao, and Y. Hu, "Model predictive control for load frequency of hybrid power system with wind power and thermal power," *Energy*, vol. 172, pp. 555–565, Apr. 2019, doi: 10.1016/j.energy.2019.01.071.

[20] X. Liu, Y. Zhang, and K. Y. Lee, "Coordinated Distributed MPC for Load Frequency Control of Power System With Wind Farms," *IEEE Trans. Ind. Electron.*, vol. 64, no. 6, pp. 5140–5150, Jun. 2017, doi: 10.1109/TIE.2016.2642882.

[21] N. Vafamand, S. Yousefizadeh, M. H. Khooban, J. D. Bendtsen, and T. Dragicevic, "Adaptive TS Fuzzy-Based MPC for DC Microgrids With Dynamic CPLs: Nonlinear Power Observer Approach," *IEEE Syst. J.*, vol. 13, no. 3, pp. 3203–3210, 2018, doi: 10.1109/JSYST.2018.2880135.

[22] S. Yousefizadeh, J. D. Bendtsen, N. Vafamand, M. H. Khooban, T. Dragičević, and F. Blaabjerg, "EKF-based Predictive Stabilization of Shipboard DC Microgrids with Uncertain Time-varying Loads," *J. Emerg. Sel. Top. Power Electron.*, 2018.

[23] B. Homayoun, M. M. Arefi, and N. Vafamand, "Robust adaptive backstepping tracking control of stochastic nonlinear systems with unknown input saturation: A command filter approach," *Int. J. Robust Nonlinear Control*, vol. 30, no. 8, pp. 3296–3313, May 2020, doi: 10.1002/rnc.4933.

[24] A. Dev, S. Anand, and M. K. Sarkar, "Nonlinear disturbance observer based adaptive super twisting sliding mode load frequency control for nonlinear interconnected power network," *Asian J. Control*, p. asjc.2364, Jul. 2020, doi: 10.1002/asjc.2364.

[25] D. Sharma and S. Mishra, "Non-linear disturbance observer-based improved frequency and tie-line power control of modern interconnected power systems," *IET Gener. Transm. Distrib.*, vol. 13, no. 16, pp. 3564–3573, Aug. 2019, doi: 10.1049/iet-gtd.2018.5855.

[26] D. Yu, W. Zhang, J. Li, W. Yang, and D. Xu, "Disturbance Observer-Based Prescribed Performance Fault-Tolerant Control for a Multi-Area Interconnected Power System with a Hybrid Energy Storage System," *Energies*, vol. 13, no. 5, p. 1251, Mar. 2020, doi: 10.3390/en13051251.

[27] Y. Yi and D. Chen, "Disturbance observer-based backstepping sliding mode fault-tolerant control for the hydro-turbine governing system with dead-zone input," *ISA Trans.*, vol. 88, pp. 127–141, May 2019, doi: 10.1016/j.isatra.2018.11.032.

[28] D. Sharma and S. Mishra, "Disturbance-Observer-Based Frequency Regulation Scheme for Low-Inertia Microgrid Systems," *IEEE Syst. J.*, vol. 14, no. 1, pp. 782–792, Mar. 2020, doi: 10.1109/JSYST.2019.2901749.

[29] S. Jain and Y. V. Hote, "Design of generalised active disturbance rejection control for delayed systems: an application to load frequency control," *Int. J. Control*, pp. 1–15, Apr. 2020, doi: 10.1080/00207179.2020.1752940.

[30] H. Haes Alhelou, M. Hamedani Golshan, T. Njenda, and P. Siano, "WAMS-Based Online Disturbance Estimation in Interconnected Power Systems Using Disturbance Observer," *Appl. Sci.*, vol. 9, no. 5, p. 990, Mar. 2019, doi: 10.3390/app9050990.

[31] C. Huang, J. Li, S. Mu, and H. Yan, "Linear active disturbance rejection control approach for load frequency control of two-area interconnected power system," *Trans. Inst. Meas. Control*, vol. 41, no. 6, pp. 1562–1570, Apr. 2019, doi: 10.1177/0142331217701539.

[32] S. Saxena, "Load frequency control strategy via fractional-order controller and reduced-order modeling," *Int. J. Electr. Power Energy Syst.*, vol. 104, pp. 603–614, Jan. 2019, doi: 10.1016/j.ijepes.2018.07.005.

[33] J.-J. E. Slotine and W. Li, *Applied nonlinear control*, vol. 199. Prentice hall Englewood Cliffs, NJ, 1991.

[34] N. Vafamand, M. H. Asemani, and A. Khayatian, "Robust L1 Observer-Based Non-PDC Controller Design for Persistent Bounded Disturbed TS Fuzzy Systems," *IEEE Trans. Fuzzy Syst.*, vol. 26, no. 3, pp. 1401–1413, Jun. 2018, doi: 10.1109/TFUZZ.2017.2724018.

[35] S. N. Sivanandam and S. N. Deepa, *Introduction to Genetic Algorithms*. Berlin, Heidelberg: Springer Berlin Heidelberg, 2008.

[36] S. Mirjalili, "Genetic Algorithm," in *Evolutionary Algorithms and Neural Networks*, vol. 780, Cham: Springer International Publishing, 2019, pp. 43–55.

[37] K. P. S. Parmar, S. Majhi, and D. P. Kothari, "Load frequency control of a realistic power system with multi-source power generation," *Int. J. Electr. Power Energy Syst.*, vol. 42, no. 1, pp. 426–433, Nov. 2012, doi: 10.1016/j.ijepes.2012.04.040.

[38] S. Velusami and I. A. Chidambaram, "Decentralized biased dual mode controllers for load frequency control of interconnected power systems considering GDB and GRC non-linearities," *Energy Convers. Manag.*, vol. 48, no. 5, pp. 1691–1702, May 2007, doi: 10.1016/j.enconman.2006.11.003.

[39] A. Safari, F. Babaei, and M. Farrokhifar, "A load frequency control using a PSO-based ANN for micro-grids in the presence of electric vehicles,"

*Int. J. Ambient Energy*, pp. 1–13, Dec. 2018, doi: 10.1080/01430750.2018.1563811.

[40] Y. Sun, N. Li, X. Zhao, Z. Wei, G. Sun, and C. Huang, "Robust H∞ load frequency control of delayed multi-area power system with stochastic disturbances," *Neurocomputing*, vol. 193, pp. 58–67, Jun. 2016, doi: 10.1016/j.neucom.2016.01.066.

**Navid Vafamand** received his B.Sc. degree in electrical engineering and M.Sc. degree in control engineering from Shiraz University of Technology, Iran, in 2012 and 2014, respectively, and Ph. D. in control engineering at Shiraz University, Shiraz, Iran, in 2019. Currently, he serves as a research assistant at Shiraz University. He was a Ph.D. Visiting student with the Department of Energy Technology, Aalborg University, Denmark, from 2017 to 2018. Dr. Vafamand is the co-author of more than 90 international conference and journal papers and four chapter books and an active reviewer in several journals. His main research interests include Takagi-Sugeno (TS) fuzzy systems, linear parameter varying (LPV) models, predictive control, and DC microgrids.

**Mohammad Mehdi Arefi** (M'17–SM'17) was born in 1982. He received the B.Sc. degree from the Department of Electrical Engineering, Shiraz University, Shiraz, Iran, in 2004, and the M.Sc. and Ph.D. degrees from the Electrical Engineering Department, Iran University of Science and Technology, Tehran, Iran, in 2007 and 2011, respectively. He is an Associate Professor with the Department of Power and Control Engineering, School of Electrical and Computer Engineering, Shiraz University. His current research interests include adaptive control, robust control, nonlinear control, system identification, and control applications in power systems.

**Mohammad Hassan Asemani** (Member, IEEE) received the B.Sc. degree from the Electrical Engineering Department, Shiraz University, Shiraz, Iran, in 2006, and the M.Sc. and Ph.D. degrees in control engineering from the Electrical and Computer Engineering Department, Tarbiat Modares University, Tehran, Iran, in 2008 and 2012, respectively. Since 2017, he has been an Associate Professor with the Power and Control Department, Shiraz University. His research interests include T-S fuzzy control, linear parameter-varying (LPV) systems, fractional-order systems, observer-based control, and linear matrix inequalities in control.

**Tomislav Dragičević** (S'09-M'13-SM'17) received the M.Sc. and the industrial Ph.D. degrees in Electrical Engineering from the Faculty of Electrical Engineering, University of Zagreb, Croatia, in 2009 and 2013, respectively. From 2013 until 2016 he has been a Postdoctoral researcher at Aalborg University, Denmark. From 2016 until 2020 he was an Associate Professor at Aalborg University, Denmark. Currently, he is a Professor at the Technical University of Denmark.

He made a guest professor stay at Nottingham University, UK during spring/summer of 2018. His research interest is application of advanced control, optimization and artificial intelligence inspired techniques to provide innovative and effective solutions to emerging challenges in design, control and diagnostics of power electronics intensive electrical distributions systems and microgrids. He has authored and co-authored more than 300 technical publications (more than 150 of them are published in international journals, mostly in IEEE), 10 book chapters and a book in the field.

He serves as an Associate Editor in the *IEEE Transactions on Industrial Electronics*, in *IEEE Transactions on Power Electronics*, in *IEEE Emerging and Selected Topics in Power Electronics* and in *IEEE Industrial Electronics Magazine*. Dr. Dragičević is a recipient of the Končar prize for the best industrial PhD thesis in Croatia, a Robert Mayer Energy Conservation award, and he is a winner of an Alexander von Humboldt fellowship for experienced researchers.